Available online at www.sciencedirect.com
SCIENCE DIRECT®
Journal of Solid State Chemistry 176 (2003) 615–632
JOURNAL OF SOLID STATE CHEMISTRY
http://elsevier.com/locate/jssc

Computational design of multifunctional materials

Nicola A. Spaldin[a,*] and Warren E. Pickett[b]

[a] *Materials Department, University of California, Santa Barbara, CA 93106-5050, USA*
[b] *Department of Physics, University of California, Davis, CA 95616, USA*

Received 16 January 2003; received in revised form 27 May 2003; accepted 24 July 2003

Abstract

We propose a general scheme for the computational design of new materials using density functional theory. We then apply the scheme to two classes of materials; ferromagnetic ferroelectrics and half-metallic antiferromagnets. Our first "designer" ferromagnetic ferroelectric has subsequently been synthesized and the predicted properties verified. Our computations on half-metallic antiferromagnets have stimulated experimental study but the phenomenon remains unconfirmed.

Keywords: Multifunctional materials; Computational design; Density functional theory; Half-metallic antiferromagnet; Ferromagnetic ferroelectric

1. Introduction

The theoretical design of materials and structures is not a new tool in Solid State Chemistry. Examples range from prediction of coordination geometries using simple considerations of radius ratios, to more sophisticated determinations of stereochemistry using the symmetry-based Woodward–Hoffmann rules [1]. Likewise, computer-aided design (CAD) has been a buzzword in the computational arena for at least two decades. Making use of the untiring capabilities of a computer to speed up many of our everyday tasks is at the root of much of the rapid change in the past half century, so its use in design is simply one of many applications. However, the computational design of materials has, until recently, been analogous to combinatorial synthesis, which speeds searches by synthesis and characterization of large numbers of samples in some automated fashion. This has allowed tremendous progress in, for example, drug design, and computational screening of molecules is now ingrained in the pharmaceutical industry. This field of application was possible because organic molecules tend to obey certain "rules" that specify bond lengths and angles, and choices and numbers of neighbors that an atom is bonded to, and such simplifications lead to semi-empirical computational methods that are accurate enough to provide the required information in many cases.

In recent years, however, developments in quantum mechanical methods such as density functional theory have combined with advances in computer hardware, to allow the prediction of new materials entirely from first principles. Such "computational materials design," sometimes also called "virtual" materials design, has been discussed in a variety of contexts [2,3]. Indeed there is even a Journal of Computer-Aided Materials Design which lists among its aims "informing the scientific community of advances in materials modelling across a spectrum of length and time scales," and "stimulating the investigation of multiscale physics, chemistry, and mechanics in understanding and utilizing materials phenomena on the electronic structure, atomistic, microstructural, and continuum levels" [4].

In this review, we concentrate specifically on ongoing efforts to design new materials with preselected functionalities using first principles computational methods. Although any scheme for computational materials design will need to be tailored to some extent to the specific problem that is being studied, a guideline, which is followed to some extent in the examples described in this paper, might be constructed as follows:

1. Clarify the functionality of interest, and determine that it is reasonable to pursue "virtual design". For example, if you need to create a material that emits

*Corresponding author.
E-mail address: nicola@mrl.ucsb.edu (N.A. Spaldin).

0022-4596/$ - see front matter © 2003 Elsevier Inc. All rights reserved.
doi:10.1016/j.jssc.2003.07.001

blue light, then your computational theory of excited states, and of the luminescence process, must be reliable enough to discern 'blue' from 'green' or 'ultraviolet'. This constraint necessarily requires that you choose your method appropriately, and that it is precise enough for your requirements.
2. Develop an understanding for the chemical conditions and physical characteristics that promote the functions to be incorporated; the objective is after all "materials design". This process will involve specifying the essential elements for success; in the examples we discuss below, we need magnetic ions with particular spin alignments, and specific (non-)conducting behavior. Stability of the material is always a consideration, although often left implicit.
3. If the class of candidate materials is large, narrow the possibilities to a subclass, described for example by crystal structure, by chemical composition, by density (if important for the functionality), etc.
4. Determine as well as possible the complexity of the problem (that is the size of the candidate pool combined with the difficulty of calculating the functionality) as it is specified to this point. "Complexity" connects the size of the pool and the difficulty of calculating the functionality. If the number of possibilities is too large, or the chance of success is too small, return to one of the previous stages and narrow the specifications or reduce the class size.
5. Choose some probable candidates, and calculate their properties. Failures may be easy to establish (perhaps the material just refuses to be ferromagnetic when that is a necessity): success requires overcoming all of the possible failures. Most likely one can never be sure—that is why we have experimentalists—but the obvious sticking points need to be addressed and superseded.
6. Feedback! Learn from your failures: respecify your class of trial materials; refine your methods or switch to a more appropriate one; check whether your "best guesses" were inappropriate.
7. When you have designed what you believe to be plausible candidates, plausible enough to justify experimental effort, persuade someone to synthesize them and characterize them well enough to check your predictions. Learn where your efforts should be improved, and back up to the appropriate step above and continue in a wiser fashion.
8. Upon success: file a patent, or better yet, write a lucid and gripping paper on the process and the success.

Almost certainly a zeroth step should have been listed: obtain a grant to support this work for a multiyear effort. Computational design of exciting and novel (multi)functional materials will not be quick or easy in the foreseeable future, but it is a concept whose time truly has come.

The remainder of this paper is organized as follows. In Section 2, we summarize the computational method—density functional theory (DFT)—that is most widely used in the computational design of new materials. Then we present two examples that illustrate the procedure: (1) a magnetoelectric multiferroic, and (2) a half-metallic antiferromagnet. In Section 4, we offer some suggestions for areas of solid state chemistry that are particularly suitable for computational design approaches.

2. Density functional theory

Since its introduction in the 1960s [5,6] DFT has evolved into a powerful tool that is widely used in condensed matter theory and computational materials for the calculation of electronic, magnetic and structural properties of solids. The method has been remarkably successful in reproducing, explaining, and in some cases predicting a wide variety of materials phenomena. Specific examples range from early predictions of phase transitions in silicon under pressure [7], to determination of stable and meta-stable adsorption geometries on metal surfaces [8], as well as many successes in understanding ferroelectric behavior and magnetic materials (both described below).

The density functional formalism is based on two theorems. First, for an interacting system of electrons in an external potential, $v(\mathbf{r})$, there exists a universal functional of the charge and spin densities, $F[\rho(\mathbf{r}), m(\mathbf{r})]$, independent of $v(\mathbf{r})$, that provides the electronic energy:

$$E = \int v(\mathbf{r})\rho(\mathbf{r})\,\mathrm{d}\mathbf{r} + F[\rho(\mathbf{r}), m(\mathbf{r})]. \tag{1}$$

Secondly, this functional takes its minimum value (the ground state energy) for the physical electron charge and spin densities [5]. (The spin density is the magnetization density in units of the Bohr magneton, μ_B.)

The density and spin polarization can be obtained from the solution of an associated single-particle problem, whose effective single-particle potential, $v_{\mathrm{eff}}[\mathbf{r}, \rho(\mathbf{r}), m(\mathbf{r})]$, is the sum of the external potential and a unique functional [6,9] of ρ and m, as presented below. As a consequence, calculation of the energy, $\rho(\mathbf{r})$ and $m(\mathbf{r})$ reduces to the self-consistent solution of a system of coupled, non-linear, one-electron-like Schrödinger equations:

$$\left[-\frac{1}{2}\nabla^2 + v(\mathbf{r}) + \int \frac{\rho(\mathbf{r}')}{|\mathbf{r}-\mathbf{r}'|}\,\mathrm{d}\mathbf{r}' + \frac{\delta E_{\mathrm{xc}}[\rho, m]}{\delta \rho_\sigma(\mathbf{r})}\right]\phi_{i,\sigma}(\mathbf{r}) = \varepsilon_{i,\sigma}\phi_{i,\sigma}(\mathbf{r}), \tag{2}$$

where σ represents up ($\uparrow$) or down ($\downarrow$) direction of the electron spin, and

$$\rho_\sigma(\mathbf{r}) = \sum_{\text{occ}} |\phi_{i\sigma}|^2, \quad m(\mathbf{r}) = \rho_\uparrow(\mathbf{r}) - \rho_\downarrow(\mathbf{r}). \tag{3}$$

The so-called Kohn–Sham wavefunctions, $\phi_{i,\sigma}$, are single-particle eigenfunctions that are strictly meaningful only for determining $\rho_\sigma(\mathbf{r})$. The Kohn–Sham eigenvalues $\varepsilon_{i,\sigma}$, which are the derivatives of the total energy with respect to the occupation of state $i\sigma$, are used in determining which one-electron states are occupied: states are filled from the lower eigenvalues to the higher, without regard to spin direction. The eigenvalues are not strictly related to single-particle excitation energies, although other theoretical considerations can explain why Kohn–Sham band structures are often a useful tool in the interpretation of spectroscopic (especially photoemission) data.

For an arbitrary density and spin polarization there is no simple explicit expression for the exchange-correlation energy, E_{xc}. The widely used local spin density approximation (LSDA) is simple, it is exact in the limit of a homogeneous electron density, and is remarkably accurate for many classes of materials. Within the LSDA, E_{xc} is written as

$$E_{\text{xc}}[\rho, m] = \int \rho(\mathbf{r}) E_{\text{xc}}[\rho(\mathbf{r}), \quad m(\mathbf{r})]\, \mathrm{d}\mathbf{r}, \tag{4}$$

where $\varepsilon_{\text{xc}}(\rho, m)$ is the exchange-correlation energy density of a uniform interacting electron gas of density ρ and spin polarization m. The LSDA is strictly justified only if $\rho(\mathbf{r})$ and $m(\mathbf{r})$ are slowly varying, and a number of extensions exist which give improved accuracy for systems with localized electrons.

Ref. [10] provides an accessible short review of the density functional method and its application to calculating the properties of solids. In addition, comprehensive discussions can be found in Refs. [11–13].

2.1. Implementations of density functional theory

One of the most widely used implementations of DFT is the so-called plane wave pseudopotential (PWPP) method [7,14], in which the Kohn–Sham wavefunctions are expanded in a basis of plane waves. Plane wave basis sets offer many advantages in DFT calculations for solids, including completeness, an unbiased representation, and arbitrarily good convergence accuracy. They also allow for straightforward mathematical formulation and implementation, which is convenient for the calculation of Hellmann–Feynman forces, [15] in density functional perturbation theory calculations [16] and for linear response calculations [17].

Plane wave basis sets do however necessitate the use of *pseudopotentials* to model the electron–ion interaction, because it not feasible to represent the rapid oscillations of the valence wavefunctions in the region around the ion cores with plane waves. The pseudopotential approximation [18] treats each nucleus plus its core electrons as a "frozen core" that does not change in response to changes in its environment. The interactions of the valence electrons with this core are then described by a pseudopotential, usually constructed from all-electron calculations to reproduce the eigenvalues, and the wavefunctions outside the core. It is implicit within the pseudopotential approach that the exchange-correlation potential, V_{xc}, like the direct Coulomb potential, is separable into a core part and a valence part:

$$V_{\text{xc}}(\rho, \sigma) = [V_{\text{xc}}(\rho, m) - V_{\text{xc}}(\rho^{\text{v}}, m^{\text{v}})] + V_{\text{xc}}(\rho^{\text{v}}, m^{\text{v}}). \tag{5}$$

Here the superscript v refers to the contribution from the valence electrons. This separation is only rigorously correct if the core electrons are spatially separated from the valence electrons, which is never exact and is certainly not a good assumption for transition metal ions, in which the *d*-electrons have substantial wavefunction amplitudes near the core region. Therefore, because V_{xc} is a non-linear function of both charge and spin polarization, use of Eq. (5) is inaccurate. A solution is offered by the partial non-linear core correction scheme [19], in which the core charge density is explicitly retained in both the construction of the ionic pseudopotential, and in the DFT calculation.

It is also possible to combine pseudopotentials with localized atomic-like basis functions rather than plane waves [20–22]. This combination offers the advantages of pseudopotentials in that only the valence electrons are treated explicitly during the self-consistent DFT calculation. In addition, the localized nature of the orbitals make the computer time and memory scale linearly with the number of atoms, and allows pseudopotentials with smaller core radii to be used, reducing the non-linear core overlap. The localized orbital basis is particularly useful for magnetic materials containing tightly bound *d*-electrons, which require a large number of plane waves to expand their wavefunctions.

In addition, all electron methods with localized basis functions, or with more intricate basis sets, such as the linear augmented plane wave (LAPW) [11] and linear muffin tin orbital (LMTO) [23] methods are also still widely used. These are more precise since they do not make the pseudopotential approximation, which in turn offers the advantage of not needing to construct a pseudopotential for each new atom to be studied. However, the most accurate all-electron methods can be considerably more computationally demanding than pseudopotential techniques.

2.2. Computer programs

There are a number of excellent computer programs available today for performing DFT calculations for

solids. These codes offer a range of methodologies, have different specialties, and are widely varying in cost (both in dollar amount and in their computer requirements). It must be emphasized that none of them should be considered "black boxes" to be used and trusted by novices—they all require a serious learning process, and the associated theoretical materials background to enable one to identify results that, on the one hand, cannot be correct or, on the other, are unexpected yet are correct.

Pseudopotential methods: Publically available codes include ABINIT [24], which allows both DFT and density functional perturbation theory calculations, Spinor [25] which extends the usual LSDA formalism to include spin–orbit coupling and generalized non-collinear magnetism and the localized basis pseudopotential program SIESTA (Spanish Initiative for Electronic Simulations with Thousands of Atoms) [20,21]. Both ABINIT and Spinor are PWPP codes and are available under the GNU General Public License [26]. SIESTA is available without charge on request to the developers. The ACRES (Adaptive Coordinate Real-Space Electronic Structure) code [27] allows either pseudopotential or all-electron calculations, and is also not planewave based. ACRES is a DFT code designed to perform total energy calculations for atoms, molecules, bulk solids and surfaces on parallel computers. The calculations are performed in real space on a grid that is adapted to spatially inhomogeneous cutoff (or resolution) requirements of a given system. For efficient use it requires a parallel computer or cluster with at least 16 processors and 4GB of memory. There are also several codes that are adapted especially for studying the dynamical behavior of solids and liquids. One is JEEP, supported at Lawrence Livermore National Laboratory [28]. Another is the Car-Parrinello molecular dynamics code CPMD, which has been applied in a wide variety of situations [29]. The Naval Research Laboratory supports the DOD planewave code [30] and the Fritz Haber Institute (Berlin) makes available its PWPP code FHImd [31].

One of the most popular "semi-commercial" PWPP codes is the VASP package [32] developed at the University of Vienna, Austria. VASP allows DFT and molecular dynamics calculations, and is quite fast because of its use of ultra-soft pseudopotentials. The developers charge a nominal fee for the source code, and require authorship on the first publication using the code.

Finally, there are also a number of fully commercialized density functional codes that are targeted in large part at chemical and pharmaceutical companies. For example, accelrys [33] markets the PWPP CASTEP code [34].

All-electron methods: Definitive studies of the predictions of DFT require all-electron, full potential electronic structure methods that include relativistic effects, of which there are now several available. The most widely used is the one based on the LAPW method, from the Vienna University of Technology called WIEN2k [35]. A small (400 Euro at press time) fee is charged to academic users. Another LAPW code of comparable accuracy is the FLEUR code [36] from Jülich, which differs mostly in the selection of features (technically referred to as "bells and whistles") that are available. In a similar vein, there is an LMTO code of Savrasov called NMO [37]. It is also all-electron, full potential, with relativistic effects included, and in addition has the capability of calculating phonons, magnons, and the electron–phonon spectral function using linear response theory. A more recent code is the full potential local orbital (FPLO) code from Dresden [38]. By using numerical local orbitals that are constrained to be relatively short range, FPLO deals with a small basis set (hence quick diagonalization) and the atomic-like orbitals also allow easier physical interpretation of results.

Finally the Stuttgart LMTO program [39] is a fast and efficient tool for calculation of charge- and spin-self-consistent band structures, partial densities of states, Fermi surfaces, total energies, and partial pressures. In addition, the program delivers tools for analyzing the electronic structure and chemical bonding such as orbital-projected band structures, crystal orbital Hamiltonian populations and electron localization functions. Since it uses the atomic sphere approximation, forces and energy differences between structures cannot be obtained accurately.

Analysis tools: Analysis tools such as electron localization functions (ELFs), crystal orbital Hamiltonian populations (COHPs), and Mulliken population analyses are included with many density functional packages, and are often immensely valuable in interpreting the results of calculations. Later in this work we describe the use of ELFs in the visualization of lone pair localization in ferroelectrics. The ELF provides a measure of the local influence of Pauli repulsion on the behavior of electrons and permits the mapping in real space of core, bonding, and non-bonding regions in a crystal [40]. It is defined as

$$\mathrm{ELF} = [1 + (D/D_h)^2]^{-1},$$

where

$$D = \frac{1}{2}\sum_i |\nabla\phi_i|^2 - \frac{1}{8}\frac{|\nabla\rho|^2}{\rho} \quad \text{and} \quad D_h = \frac{3}{10}(3\pi^2)^{5/3}\rho^{5/3}.$$

Here ρ is the electron density and ϕ_i are the Kohn–Sham wavefunctions.

3. Two design examples

In this section, we describe two classes of "designer materials" for which predictions have been made using DFT. The first, a ferromagnetic ferroelectric, has subsequently been synthesized and the predicted properties verified. The second prediction, of a half-metallic antiferromagnet, has stimulated experimental study but remains unconfirmed.

3.1. Design of a magnetoelectric multiferroic

A multiferroic is a material in which two or all three of ferroelectricity, ferromagnetism and ferroelasticity occur in the same phase [41]. The "ferro" designation describes a broken symmetry, and a related character, that can be aligned by application of an appropriate field: spontaneous magnetization, reoriented by an applied magnetic field; electric polarization, reoriented by an electric field; and spontaneous deformation, which can be reoriented by an applied stress. Perhaps the use of the term multiferroic should be broadened to include "ferroconductivity" (i.e., superconductivity), especially since coexisting superconductivity and ferromagnetism have been reported recently in $RuSr_2GdCu_2O_8$ [42], UGe_2 [43] and URhGe [44]. Intriguing theoretical and experimental questions that this unexpected coexistence raises are now attracting much study [45,46]. The spontaneously broken symmetry of the "ferroconductor" is not so evident or so simple to describe, but its divergent ("infinite") response to electric and magnetic fields place it in the same general category.

The coupling between ferroelectricity and ferroelasticity is well established, and leads to the widespread use of ferroelectric materials in transducer applications [47]. Similarly the coupling between ferromagnetism and ferroelectricity results in magnetoelectricity and the manipulation of magnetic behavior by electric fields and vice versa. These latter effects are not well studied, due to the dearth of ferromagnetic ferroelectric materials. In this section, we describe the design and subsequent synthesis of such a magnetoelectric multiferroic. Part of our motivation is the range of new applications that can be envisaged [48]. First, the ability to couple either to the electric or the magnetic polarization might allow an additional degree of freedom in the design of conventional actuators, transducers and storage devices. Other potential applications include multiple state memory elements, in which data is stored both in the electric and the magnetic polarizations, or novel memory media which might allow writing of a ferroelectric data bit, and reading of the magnetic field generated by association. Aside from the potential applications, the fundamental physics of multiferroic magnetoelectrics is rich and fascinating.

3.1.1. Understanding the origin of ferromagnetism and ferroelectricity

What causes ferroelectricity? A ferroelectric is a material that undergoes a phase transition from a high-temperature phase which behaves as an ordinary dielectric (in which an applied electric field induces an electric polarization proportional to the field, which reverts to zero when the field is removed) to a low-temperature phase which has a spontaneous polarization, whose direction can be switched by an applied field. There has been a great increase in the understanding of the fundamental physics of ferroelectrics over the last 10 years [49], and first principles DFT calculations have contributed significantly to our current understanding of the origin of ferroelectric behavior. Theoretical developments that allow the calculation of the ferroelectric polarization have also occurred during this time period [50–52].

The most widely studied and widely used ferroelectrics today are perovskite structure oxides, ABO_3, which have the prototypical cubic structure shown in Fig. 1. The cubic perovskite structure is characterized by a small cation, B, at the center of an octahedron of oxygen anions, with large cations, A, at the unit cell corners. Below the Curie temperature, there is a structural distortion to a lower symmetry phase accompanied by the shift off-center of either the A or B cations (or both) relative to the oxygen anions. The spontaneous polarization derives largely from the electric dipole moment created by this shift.

If the bonding in an ideal cubic perovskite were entirely ionic it would remain centrosymmetric (and therefore not ferroelectric), because the short-range repulsions between adjacent closed shell ions are

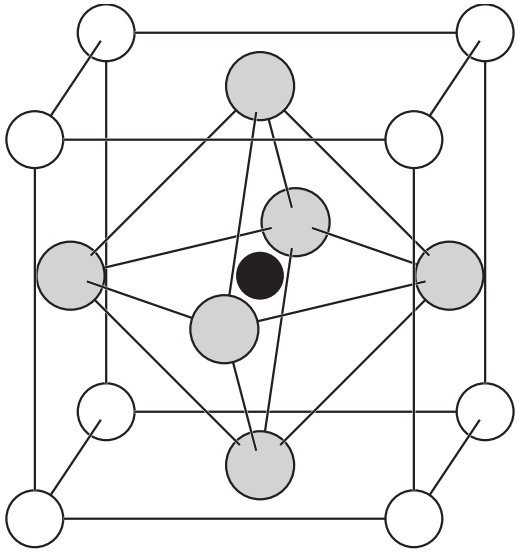

Fig. 1. The cubic perovskite structure. The small B cation (in black) is at the center of an octahedron of oxygen anions (in gray). The large A cations (white) occupy the unit cell corners.

minimized for symmetric structures. The existence or absence of ferroelectricity is determined by a *balance* between these short-range repulsions, which favor the non-ferroelectric symmetric structure, and additional bonding considerations which act to stabilize the distortions necessary for the ferroelectric phase. Currently two distinctly different chemical mechanisms for stabilizing the distorted structure in common ferroelectrics have been identified. Both are described as second-order Jahn–Teller effects in the chemistry literature, see, for example, Ref. [53].

The first mechanism is the ligand field stabilization of a transition metal cation by its surrounding anions, arising from the off-center displacement of the small cation in the common perovskite ferroelectrics such as $BaTiO_3$ and $Pb(Zr,Ti)O_3$. The behavior was studied within DFT [54,55] in $PbTiO_3$ and $BaTiO_3$ and the ferroelectric distortion was ascribed to Ti $3d$–O $2p$ hybridization. It is significant for the discussion of multiferroic materials that the Ti^{4+} ion is formally in a "d^0" state so that the lowest unoccupied energy levels are d-states which tend to hybridize with O $2p$ ions [61,62]. Most other perovskite ferroelectrics also contain d^0 B cations, such as Zr^{4+} and Nb^{5+}.[1]

The second mechanism focuses on "lone pair" cations which have a formal ns^2 valence electron configuration. In the same vein as the d^0 ions discussed above, these ions can be described as "p^0" ions. The formally d^0 ions actually contain some d charge density that hybridizes with oxygen $2p$ ions during ferroelectric distortions. Likewise the p^0 ions contain some p charge density which contributes to displacive distortions. Indeed the tendency of ns^2 ions to lose inversion symmetry is well established, with the conventional explanation invoking a mixing between the ns^2 ground states and a low-lying ns^1 np^1 excited state, a mixing that can only occur if the ionic site does not have inversion symmetry [56]. If the lowering in energy associated with the mixing is larger than the inter-ionic repulsion opposing the ion shift, then a distortion results. This "stereochemical activity of the lone pair" is the driving force for off-center distortion in the group IV chalcogenides [57] (for example GeTe). Sometimes both mechanisms occur in the same material, for example in $PbTiO_3$, where the activity of the lead ion causes a strain which stabilizes the tetragonal phase over the rhombohedral phase seen in $BaTiO_3$ [55].

What causes ferromagnetism? A ferromagnetic material is defined as one which undergoes a phase transition from a high-temperature phase which does not have a macroscopic magnetic moment, to a low-temperature phase which has a spontaneous magnetization even in the absence of an applied magnetic field. There are two phenomenological theories of ferromagnetism which have been successful in explaining many of the properties of ferromagnets, and other kinds of magnetic ordering—the Curie–Weiss localized moment theory arising from the study of magnetic insulators, and the Stoner band theory of ferromagnetism in metals. We summarize these models below, and show that, in both cases, tightly bound, localized electrons, such as transition metal d, or rare earth f electrons, provide the impetus for magnetism to occur.

In a classic 1907 paper [58], Weiss postulated that an internal "molecular field" acts in ferromagnetic materials to align magnetic moments, arising from unequal numbers of $\uparrow$ and $\downarrow$ spin electrons localized on each atom or ion, parallel to each other. Today we understand the origin of the Weiss molecular field to arise, not from the long-range dipolar interaction envisioned originally, but rather from the short-range quantum mechanical exchange energy, which causes electrons with parallel spins (and therefore parallel magnetic moments) to have a lower energy than electrons with antiparallel spins, all other factors being equal. Below the Curie temperature, T_c, the molecular field is so strong that it magnetizes the substance even in the absence of an external applied field. At high enough temperatures, the thermal energy, kT, and associated entropic effects overcome the alignment energy of the molecular field, resulting in random orientation of the magnetic moments and paramagnetic behavior. The Weiss picture leads to the experimentally observed Curie–Weiss law behavior for the susceptibility, χ, of many magnetic materials:

$$\chi = \frac{C}{T - T_c} \tag{6}$$

and also accounts for the observed susceptibility of many antiferromagnets (AFMs) and ferrimagnets.

The Weiss theory breaks down in one important aspect, however—it is unable to account for the measured values of the magnetic moment per atom in some ferromagnetic materials, particularly in ferromagnetic metals. There are two significant discrepancies. First, according to the Weiss theory, the magnetic dipole moment on each atom or ion should be the same in both the ferromagnetic and paramagnetic phases. Experimentally this is not the case. Second, in local moment theory, the magnetic dipole moment on each atom or ion should correspond to an integer number of electrons. Again this result is often not observed. A more successful approach is to use the Stoner band theory of ferromagnetism [59], in which the fundamental driving force for ferromagnetism is again the exchange energy, which is minimized if all the electrons have the same spin. Opposing the alignment of spins is the increased band energy involved in transferring electrons

[1] We emphasize again that the presence or absence of ferroelectricity is determined by a balance between effects. For example, chemically similar $BaTiO_3$ and $SrTiO_3$ show quite different behavior.

from the lowest band states (occupied equally with up- and down-spin electrons) to band states of higher energy. This band energy prevents simple metals from being ferromagnetic.

For example, in the elemental ferromagnetic transition metals, Fe, Ni, and Co, the Fermi energy lies in a region of overlapping 3*d* and 4*s* bands. The 4*s* bands are broad, with a low density of states at the Fermi level. Consequently, the energy which would be required to promote a 4*s* electron into a vacant state so that it could reverse its spin is more than that which would be gained by the resulting decrease in exchange energy, and so the 4*s* bands are not spin polarized. By contrast, the 3*d* band is narrow and has a much higher density of states at the Fermi level. The large number of electrons near the Fermi level reduces the band energy required to reverse a spin, and the exchange effect dominates. The exchange interaction produces an exchange potential that effectively shifts the energy of the 3*d* band for electrons with one spin direction relative to the band for electrons with the opposite spin direction, giving the exchange-split band structure shown in Fig. 2. The magnetic moment does not necessarily correspond to an integer number of electrons, since the electrons are shared between partially filled 4*s*, $3d^{\uparrow}$ and $3d^{\downarrow}$ bands. In *d* band metals with other kinds of magnetic ordering (such as antiferromagnetic), the same phenomenology explains the existence of the magnetic moments, although additional factors are responsible for the different ordering.

Real materials obviously do not behave exactly like either of these simple models, although one or other is usually a fairly reasonable description in most cases. For example, rare earth magnets contain highly localized *f* electrons which are well described by the Weiss localized moment theory, whereas in metallic ferromagnets the magnetic order, arising from the less strongly localized *d* orbitals, is Stoner band-like. The cases in which magnetism arises from orbitals other than localized *d* or *f* electrons are rare, and we will restrict our search to conventional Stoner-like or Weiss-like materials, in which narrow bands with localized electrons provdie the magnetism, in this example. We note that, in practice, methods such as DFT do not assume a particular model type, but rather describe the system from first principles, and are the best options for calculating the properties of magnetic materials [60].

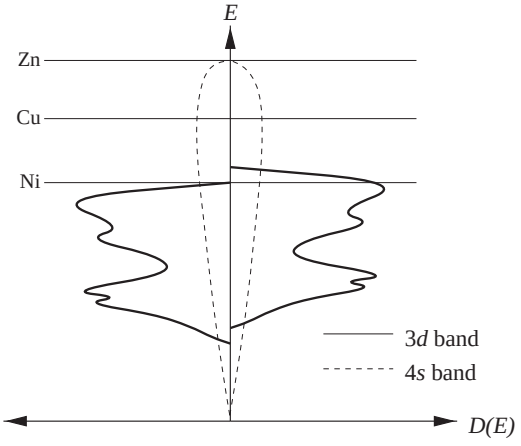

Fig. 2. Schematic 3*d* and 4*s* up- and down-spin densities of states in first row transition metals, with exchange interaction included.

Other restrictions: Finally, we point out that all physical, structural and electronic properties of magnetoelectric multiferroics are restricted to those which occur both in ferromagnetic and in ferroelectric materials. So the symmetry of the crystal is restricted to one of the 13 point groups (1, 2, $2', m, m', 3, 3m', 4, 4m'm', m'm2', m'm'2', 6$ and $6m'm'$) that allow both spontaneous electric polarization and spontaneous magnetic polarization. Also, by definition, a ferroelectric material must be an insulator (otherwise an applied electric field would induce an electric current to flow, rather than causing an electrical polarization). Therefore, our search is restricted to the class of magnetic insulators. This class is quite small, which limits the possibilities drastically; this can be a welcome focus, or a frustrating limitation, depending on the point of view.

3.1.2. Choosing a trial magnetoelectric multiferroic

We showed above that the common perovskite oxide ferroelectric materials necessarily have a formal charge corresponding to the d^0 electron configuration on the *B* cation. This d^0-ness favors ferroelectricity because of a ligand field stabilization in which the formally filled oxygen 2*p* states donate electron density into the formally empty *d* states of the transition metal cation as it moves off-center [54,61]. Clearly, vacant transition metal *d* states in an appropriate energy range are required for such stabilization to occur. We also pointed out above that the occurrence of magnetic spin polarization on the transition metal is subject to the *opposite* requirement—there must be localized electrons, which are provided by filled transition metal *d* states. Therefore, the existence of ferroelectricity by the conventional off-centering of the *B* cation (which requires empty *d* orbitals) is inconsistent with the occurrence of spin polarization on the transition metal (which requires filled *d* orbitals).

We therefore have two options for designing a ferromagnetic ferroelectric. The first is to retain the d^0 *B* cation for providing the ferroelectricity, and introduce a rare earth with a partially filled *f* shell onto the *A* cation site. However, the large distance between the strongly localized *f* electrons would likely give rise to paramagnetic ordering in this case. The second option is to allow the *B* cation to be magnetic (and therefore not ferroelectric) and introduce a cation with a stereoche-

mically active ns^2 lone pair on the A-site. We pursue this latter route here.

The following common ions have an ns^2 electron configuration: Ge^{2+} $(n=4)$, Sn^{2+} $(n=5)$, and Tl^{+}, Pb^{2+}, Bi^{3+} $(n=6)$. However, the fourth $(4s^2)$ and fifth $(5s^2)$ row ions are too small to stabilize the A-site in perovskite ferroelectrics. Of the sixth row elements, Tl tends to form pyrochlores, and also tends to adopt the +3 oxidation state (which does not have a lone pair). For example, $Tl_2Mn_2O_7$ is of interest as a ferromagnetic pyrochlore, but has no driving force for ferroelectricity. Pb^{2+} is well known to be an active A-site ferroelectric ion in the perovskite structure, and there are also a number of magnetic double perovskites and magnetic pyrochlores containing Pb^{2+}. Bi^{3+} is less well studied but is also able to occupy the A-site in perovskite ferroelectrics.

A literature search of Bi-based perovskites revealed $BiFeO_3$ to be the only $BiXO_3$ compound (X = trivalent transition metal) that has been studied in any detail. It is known to be ferroelectric below 1110 K, and antiferromagnetic with a Néel temperature of 670 K [63]. It shows the linear magnetoelectric effect, with applied magnetic fields inducing weak ferromagnetism and large increases in polarization [64]. Note that the Fe^{3+} ion in $BiFeO_3$ has the d^5 electron configuration, and therefore is not a d^0 ion, therefore the ferroelectricity is almost certainly driven by stereochemical activity of the Bi^{3+} lone pair.

Before the theoretical work described in this paper was carried out, there had been no measurements of ferroelectricity in other Bi-based perovskites. $BiCrO_3$ (in which the formally Cr^{3+} ion has three $3d$ electrons) was reported in a 1968 paper to be antiferromagnetic with a weak ferromagnetic moment below 123 K [65]. A high temperature structural phase was reported to be pseudomonoclinic with lattice parameters $a=c=3.878$ Å, $b=7.765$ Å and $\beta=88°50'$. Superstructure lines were observed, and could be assigned to a unit cell doubled along the b direction, with adjacent Bi^{3+} ions shifted in opposite directions, suggesting a possible antiferroelectric phase. Little was known about $BiCoO_3$ and $BiNiO_3$ (d^6 and d^7 on the Co^{3+} and Ni^{3+} ions, respectively) beyond the fact that they form in the cubic perovskite structure, but $BiCo_{0.5}Fe_{0.5}O_3$ was known to be ferromagnetic [66], probably because of a double-exchange-type mechanism between neighboring d^6 and d^5 ions. Bismuth manganite, $BiMnO_3$ [67] was also known to be ferromagnetic, with a triclinic structural distortion in its ground state. The ferromagnetism is unexpected, because, like the rare-earth manganites, $BiMnO_3$ has trivalent Mn cations with four $3d$ electrons. The four $3d$ electrons should in all cases drive a Jahn–Teller distortion of the surrounding oxygen octahedra, which, combined with the super-exchange interaction, should cause antiferromagnetic magnetic symmetry [68], as is indeed observed in the rare-earth manganites. In fact a number of researchers suggested in informal discussions, that the observed ferromagnetism was likely the result of oxygen non-stoichiometry in the samples causing double-exchange-like interactions.

Based on the reported observation of ferromagnetism in $BiMnO_3$, and of ferroelectricity in $BiFeO_3$, we chose $BiMnO_3$ as our candidate ferromagnetic ferroelectric for further study.

3.1.3. *Calculation of the properties of* $BiMnO_3$ *using density functional theory*

In this section, we review the series of studies that constituted the first-principles density functional prediction of ferroelectricity in $BiMnO_3$, and the subsequent explanation of the origin of the ferroelectricity. A range of DFT implementations were used in the calculations described here, including the CASTEP [34] and ABINIT [24] plane wave pseudopotential programs, the Stuttgart-LMTO package [23] and the SIESTA code [22]. All results were obtained using the local spin density approximation.

Ferroelectric Instability? The first modern theoretical study of $BiMnO_3$ was by Hill and Rabe [69], who calculated the zone center phonon modes of cubic $BiMnO_3$ in order to determine the existence and nature of ferroelectric instabilities. The dynamical matrix was determined by calculating the Hellmann–Feynman forces resulting from the displacement of each atom in turn 0.1 Å along the z direction of the unit cell. It was then diagonalized to obtain the phonon eigenvalues and eigenvectors. Non-centrosymmetric optical phonons with imaginary eigenvalues are indicative of off-center lattice instabilities that might be ferroelectric, unless over-ridden by a stronger instability elsewhere in the Brillouin zone.

The ferromagnetic cubic phase of $BiMnO_3$ was found to have one unstable zone center phonon mode corresponding to a ferroelectric distortion. As expected, the ferroelectric mode consisted of the Bi cation moving in opposition to the oxygen cage, creating a Bi–O electric dipole moment.

Band structure analysis: Hill and Rabe [69] also calculated and analyzed the DFT band structure of $BiMnO_3$ in order to further understand the nature of the Bi–O interaction. Fig. 3 shows the band structure of $BiMnO_3$ in its cubic paramagnetic phase, plotted along the high symmetry axes of the simple cubic Brillouin zone. The Fermi level is set to zero. The broad series of bands between −2 and −7 eV arises from the oxygen $2p$ orbitals. Above the oxygen $2p$ bands, and hybridized with them, are the Mn $3d$ bands. The Mn $3d$ bands are divided into two sub-bands—the lower energy t_{2g} bands, and the higher energy e_g bands—as a result of crystal field splitting by the octahedral oxygen anions. The Fermi level lies near the top of the Mn $3d$ t_{2g} bands and

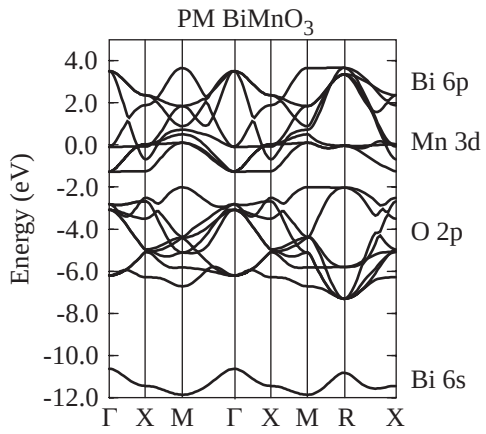

Fig. 3. Calculated band structure for cubic paramagnetic $BiMnO_3$ along the high symmetry axes of the Brillouin zone.

is in a region of fairly flat bands and therefore high density of states. When the system is allowed to relax to its ground magnetic and structural state, a gap opens and an insulator is formed, as required for a ferroelectric [70]. Note the presence of a band between −10 and −12 eV in the $BiMnO_3$ band structure corresponding to the high lying occupied Bi 6*s* electrons, and the Bi 6*p* bands intersecting the Fermi energy.

A tight-binding analysis of the $BiMnO_3$ band structure found that the inclusion of Bi–O interactions is necessary to reproduce the ab initio bands. The largest transfer integrals involving Bi were found to be the Bi 6*s*–O 2*p* and Bi 6*p*–O 2*p* σ interactions, with the magnitude of the σ-bonded Bi 6*p*–O 2*p* interaction being approximately 30% larger than that of the Bi 6*s*–O 2*p*.

Stereochemical activity of the Bi lone pair: Finally, Seshadri and Hill [70] provided a visualization of the role of the $6s^2$ lone pair in driving the low symmetry distortion of $BiMnO_3$ by calculating the first principles electronic properties of $BiMnO_3$ in its *experimentally observed* monoclinic structure using the DFT LMTO method. By comparing the properties of monoclinic $BiMnO_3$ with those of the undistorted cubic perovskite phase, and with $LaMnO_3$, in which no lone pair is present, they showed that the lone pair drives the off-center distortion in monoclinic $BiMnO_3$ and in turn causes its novel multiferroic properties.

Fig. 4 compares the ELFs projected onto the A–O and Mn–O planes of $BiMnO_3$ and $LaMnO_3$, constrained in the ideal cubic perovskite structure. In Fig. 4, the Mn is at the center of the unit cell and the large cations are at the corners. The color scheme is shown in the bar accompanying the images, with deep blue signifying one extreme of almost no localization (nearly free electrons) and white signifying regions where electrons are completely localized. Note first that the ELFs in the Mn–O plane are very similar for the two compounds, suggesting that the different magnetic

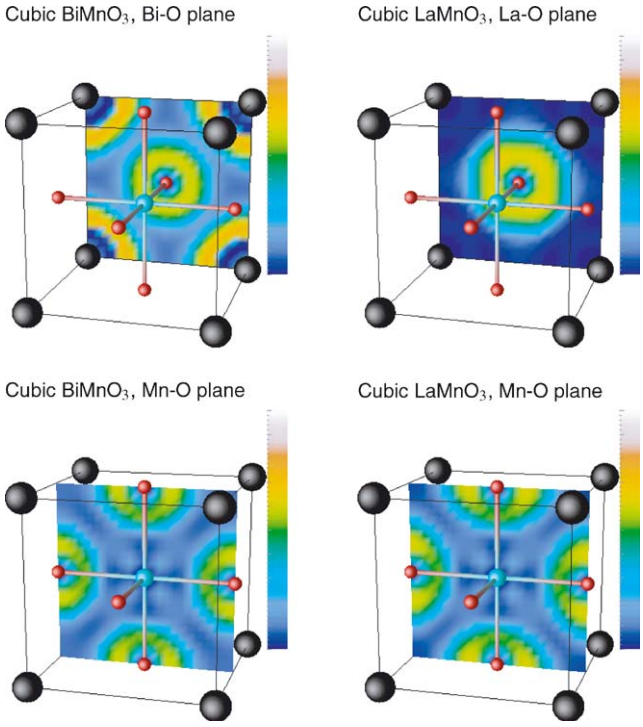

Fig. 4. Valence ELFs in the A–O and Mn–O planes of the cubic structures of $BiMnO_3$ and $LaMnO_3$. The perovskite *A* atom (Bi or La) is in the corner of the cell and the *B* atom (Mn) is at the center, six-coordinate with O. See Ref. [70].

orderings observed experimentally in $LaMnO_3$ and $BiMnO_3$ are the result of their different ground state *structures*, rather than in changes in the Mn–O interactions. However, large differences can be seen in the A–O planes. In particular, regions of spherical charge localization corresponding to the filled 6*s* shell can be seen around the Bi atoms. In contrast the ELF around the La atoms in $LaMnO_3$ indicates almost zero electron localization.

Fig. 5 shows a real space depiction of the stereochemistry of the lone pair in monoclinic $BiMnO_3$, from Ref. [70]. The ions are fixed at the experimental coordinates of Ref. [71], and a ferromagnetic ground state, with a magnetization of 4 μ_B per formula unit, is found. The striking yellow lobe-like regions in the isosurface correspond to the Bi lone pair that is able to adopt a traditional lone-pair geometry in the distorted monoclinic structure. Seshadri and Hill concluded that the transformation from a nearly spherical lone-pair in the cubic phase to a lobe-like lone pair in the monoclinic phase is likely a significant driving force for structural distortion in this system. Note that the charge density within the localized lone-pair lobe contains a significant contribution from the oxygen 2*p* electrons, consistent with the large Bi–O 2*p* hybridizations found in the tight-binding analysis. The involvement of the ligand is not included in the "text book" picture of a lone pair, in

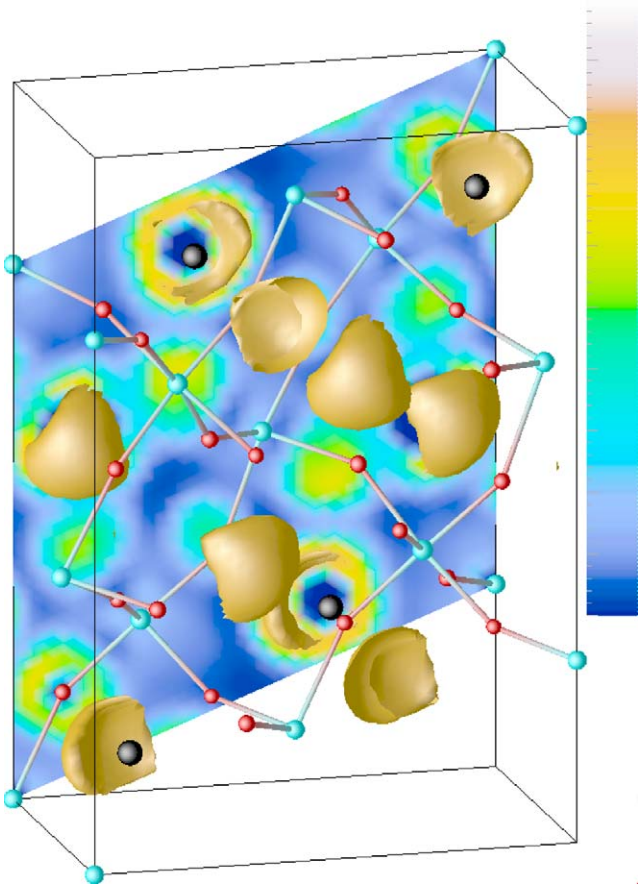

Fig. 5. Isosurface (at a value of 0.75) of the valence electron localization function of $BiMnO_3$, calculated at its experimental structure. The projection on the back face of the cell shows the valence electron localization function, color coded as in the bar by the side of the figure. The crystal is oriented slightly off the *b*-axis (from Ref. [70]).

which the off-centering is usually attributed to mixing with the *p* states on the *same* ion [72].

3.1.4. *Synthesis and characterization of* $BiMnO_3$

Subsequent to the commencement of the theoretical work described in this section there have been a number of experimental studies on both polycrystalline bulk samples [71,73–75] and thin films [74,76] of $BiMnO_3$. Two particularly important results have emerged from these experiments. The first is the observation of ferroelectric hysteresis below 400 K both in bulk polycrystalline samples [74] confirming the DFT prediction. The hysteresis was observed to persist down to the lowest temperature measured (80 K), confirming that the ferromagnetic and ferroelectric regions indeed coexist. Above 400 K the samples showed too much hopping conductivity to sustain an electric polarization; however, a structural phase transition at 450 K was suggested to be the ferroelectric to paraelectric phase transition. This is, to our knowledge, the first ab initio prediction and subsequent synthesis of a new ferroelectric material.

The second fascinating experimental finding is the result of detailed analysis of the neutron diffraction data to reveal the nature of the ferromagnetic ordering in $BiMnO_3$ [71,75]. As in the conventional rare-earth manganites, each MnO_6 octahedron is elongated along one axis as a result of the Jahn–Teller distortion around the d^4 Mn^{3+} ion. Orbital ordering then leads to four singly occupied d_{z^2} orbitals pointing towards empty $d_{x^2-y^2}$ orbitals on adjacent Mn ions (a ferromagnetic interaction [68]) and two empty $d_{x^2-y^2}$ orbitals pointing towards other empty $d_{x^2-y^2}$ orbitals (an antiferromagnetic interaction). In $LaMnO_3$, the four ferromagnetic interactions align in planes, with antiferromagnetic interactions between them, leading to the observed *A*-type antiferromagnetic ordering shown in Fig. 6(a). This type of ordering minimizes the stress in the system, since the shorter antiferromagnetic bonds all lie in the same plane. In $BiMnO_3$, however, the large distortion introduced by the Bi lone pair, over-rides the tendency for the short bonds to align in a plane, and the orbital ordering is three dimensional (Fig. 6(b)). Thus, the structure is ferromagnetic, although still frustrated, (since two of the Mn–Mn interactions would like to be antiferromagnetic).

In summary, the stereochemically active lone pair in $BiMnO_3$ causes a symmetry lowering structural distortion which both drives the ferroelectric phase transition, and, as a secondary effect, allows ferromagnetic ordering.

3.2. *Design of a half-metallic antiferromagnet*

To discuss the design of a half-metallic antiferromagnet (HM AFM), two basic concepts have to be introduced. The first is that of an HM FM; the second is the (slightly misnamed) half-metallic *anti*ferromagnet. Confining ourselves to the simplest situation of stoichiometric compounds, where electron transport is readily categorized—metallic, or insulating—the vast majority of ferromagnetic materials are metallic. Many of the few ferromagnetic insulators that are known are under current study to understand the microscopic mechanism for spin alignment, because the common state of affairs is for magnetic insulators to be AFMs.

In a ferromagnet, the majority ('spin up') and minority ('spin down') electronic systems (also called channels) have distinct band structures, which in the simplest picture are identical bands split by the exchange splitting Δ_{ex}. As a result, not only is the material magnetic (because the bands are filled with different numbers of electrons) but its electric current is spin polarized (unbalanced) because the band structures are different at the Fermi level. In practice, the band structures can be considerably more complicated,

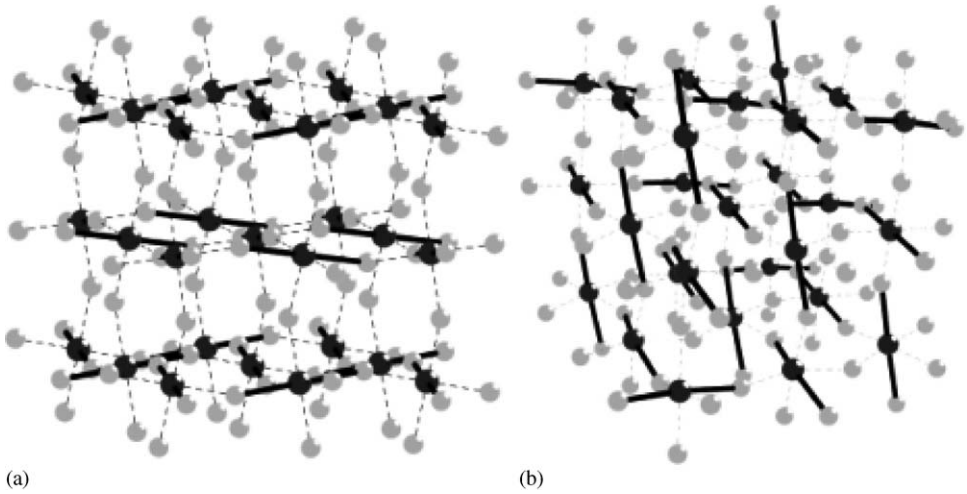

Fig. 6. The two-dimensional orbital ordering in $LaMnO_3$ (a) is compared with the three-dimensional orbital ordering in $BiMnO_3$ (b). The bold lines represent the orientation of the d_{z^2} orbitals, as revealed by elongations of the MnO_6 octahedra. From Ref. [75]. Copyright (2002) by the American Physical Society.

however, and it is altogether possible that there is a gap in the bands of one spin channel (hence 'insulating') while there is none in the other channel, leaving it metallic, conducting, and displaying a Fermi surface. In this case, the conduction is 100% spin polarized, a unique signature of a half-metal. Another signature is that the spin magnetic moment is an integer: the spin channel with a gap will have an integer number $N_\uparrow$ of filled bands, holding $N_\uparrow$ electrons per cell. This leaves the other spin channel with an integer number $N_\downarrow$ of electrons (since we are restricting our consideration to stoichiometric compounds with an integer number of electrons in each cell). The spin magnetic moment, in μ_B, is the difference of the two integers: $\mathscr{M} = N_\uparrow - N_\downarrow$.[2] A semi-popular description of half-metals and their projected applications has recently appeared [78].

To make short what could be a much longer tale: the material can be magnetic and yet the integer $\mathscr{M}$ can be zero [79]. This requires more than one magnetic atom (or ion) in the cell, directed ↑ and ↓ in such a way that their equal but inequivalent moments cancel. A schematic density of states for a simple HM AFM is shown in Fig. 7, where it is compared to a simple model of an HM FM. The original suggestion for an HM AFM material was the Heusler-like quintinary ordered alloy $V_7MnFe_8Sb_7As$ [79]. Unfortunately, due to the complexity and intricacy of the unit cell, and to the intermetallic nature of the constituents, there is no expectation that the ordered version of this material can actually be realized in the laboratory (achieving good order in much simpler systems is often difficult to achieve). It must be recognized that a true antiferromagnetic *cannot* fulfill the requirements of being half-metallic. In a true AFM, the bands for each spin direction are equivalent, by symmetry, but the bands cannot be equivalent in an HM AFM, because one direction has a gap, and the other does not, at the Fermi level. The simplest way to achieve the required state of affairs for an HM AFM is to have a unit cell with two

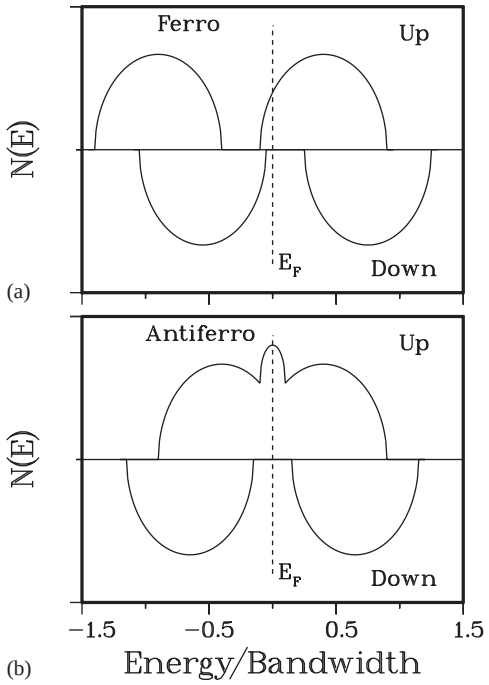

Fig. 7. Model density of states for a half-metallic ferromagnet (a) and a half-metallic antiferromagnet (b). ↑(↓) density of states is plotted upward (downward). For the HM FM, ↑ and ↓ DOS are identical except for an exchange splitting that lowers the ↑ states. For the HM AFM, the exchange splitting is of opposite sign for the bands at low and high energy. Both ↑ and ↓ bands are symmetric around the zero of energy, hence the net moment vanishes.

[2] Spin–orbit coupling makes these specifications less precise, but we will confine ourselves to atoms where spin–orbit effects are small.

different magnetic ions, ions which have the same moment but which are anti-aligned, viz. Cu^{2+} $S=\frac{1}{2}\uparrow$, and V^{4+} $S=\frac{1}{2}\downarrow$. The concept, and possible realization, should become clearer as the process of designing an HM AFM is described.

The properties of an HM AFM are highly unusual—basically, an HM AFM achieves the properties of an HM FM, but in a material with vanishing macroscopic magnetization, in spite of the strong internal exchange field. This distinction can be very important in spintronics applications, where an HM AFM would have the properties of the standard half-metal (specifically, 100% spin-polarized current) but would be impervious to magnetic fields. The properties, most of them shared by the HM FM and the HM AFM, are: (a) magnetic order below an ordering temperature (''Curie'' is more appropriate than ''Néel'') T_c; (2) half-metallicity, that is, one spin channel is metallic, and the other is gapped, so the Fermi surface is composed of carriers of only one spin direction, and conduction is 100% polarized; (3) the magnetic moment vanishes (at least at $T=0$, which is all we discuss here), in spite of having the symmetry of a ferromagnet; (4) the spin (Pauli) susceptibility vanishes, and the spin-lattice relaxation time is infinite, both for the same reason—there are no low energy spin-flip transitions available to the system. An applied magnetic field shifts the $\uparrow$ bands with respect to the $\downarrow$ bands, but there is no change in the magnetization. To oversimplify only a little: the charge excitations are typical of a metal, while the spin-flip spectrum is that of an insulator.

Other properties follow straightforwardly from these, but can be highly provocative—for example, one of the possibilities driving the search for an HM AFM was the realization that it could become superconducting, but would be an extremely unusual, *single spin* superconductor [80,81]. There are unsettled questions about the behavior of an HM AFM at non-zero temperature; Irkhin and Katsnelson have suggested that the properties will differ from those of an ordinary Fermi liquid. [82]. The HM FM has also raised new and interesting questions about spin DFT, some of which have been settled [83].

3.2.1. Choice of structural class

For any solid state scientist, whether chemist or physicist, classification by crystal structure type is one of the most fundamental and important. ''Type'' generally infers a classification with respect to unit cell constituents and bonding characteristics: $CaTiO_3$ and $MgCNi_3$ both have the perovskite crystal structure, but their chemistry (and properties—ionic insulator versus metallic superconductor) are so different that it would be counterproductive to include them in the same *crystal structure type*.

To choose a structure type within which to search and design, familiarity and scientific understanding must get great consideration, since these will provide guidelines on whether the desired functionality is likely to arise within that class. At least in early stages, one should also strive for simplicity. For the HM AFM, which requires two distinct magnetic atoms (ions) in the cell and the likelihood of both metallic behavior and energy gaps, one obvious choice would be the transition metal monoxides, $TO \rightarrow TT'O_2$, i.e., an ordered 50-50 'alloy' of two transition metals T and T' to form a supercell. Transition metal monoxides tend to have large bandgaps and display strongly correlated behavior, however, which makes them a poor choice for a beginning study. Intermetallic compounds, as mentioned above, often do not order well, and non-stoichiometry introduces complications that should be avoided if possible. A combination of magnetic ions and metalloids might be viable. For the first study, however, the perovskite structure was chosen, as it has numerous members (a positive feature but also a complication), it has been studied for decades and much is understood, and finally there are ''more than 300'' *double perovskites* known [84]. Introducing two magnetic ions in an ordered fashion into the perovskite structure leads, in the simplest case, to this double perovskite structure.

3.2.2. Combinatorial aspects

Anderson et al. listed a decade ago 300+ double perovskite known materials [84]. This number has increased since, partially because HM FMs have been found (and substantiated experimentally, to some degree) first in the ''colossal magnetoresistance'' manganese oxides with perovskite structure [85], and secondly in some double perovskite compounds, most notably Sr_2FeMoO_6 [86]. However only about 5% of the 300 compounds contained a magnetic ion. Two questions arise: how many choices are there, and how does one make good selections among the choices?

Let us first consider the class $La_2TT'O_6$, where T and T' are distinct transition metal ions. What are the number of such pairs? Such ions are characterized by a nominal d^n configuration where $1 \leqslant n \leqslant 9$. Since each such configuration can be realized by more than one ion (in different charge states), and there are several uni-, di-, and trivalent cations A to choose from, there are thousands of magnetic double perovskite compounds that might be considered. Supposing on average that each ion has two common charge states, and there are three rows of transition metals, there are $9 \times 3 \times 2 = 54$ ions, and hence $54 \times 53/2 \approx 1400$ ion pairs. The cation of course need not be La, it could be Ca or Sr or Y, or one of perhaps 20 ions including rare earths and possibly some actinides. This leads to $\sim 30\,000$ potential double perovskite compounds with magnetic ions, no more than ~ 25 of which have been reported. Moreover,

the two A-site cations could be distinct, increasing the number by another order of magnitude or more.

A rational computational search/survey of this number of systems would be hopeless. Fortunately, there is chemistry, physics, and good sense to narrow the possibilities drastically. The first restriction is charge balance: in the $La_2TT'O_6$ class of materials, for example, the experience of solid state chemists tells us that the sums of the formal charges Q, Q' on the magnetic ions must satisfy $2\times(+3)+Q+Q'+6\times(-2)=0$, or $Q+Q'=6$. This limits the choices to $(3+,3+)$, $(4+,2+)$, and $(5+,1+)$ pairs. This restriction greatly reduces the number of possibilities. In addition, there are few 5+ ions, and a limited number of 4+ ions, reducing the list even further (Table 1).

3.2.3. Anticipated magnetic moments

Charge balance (from solid state chemistry) narrows the number of choices considerably, but there is more narrowing that can be carried out using solid state physics, since one can estimate an ion's spin, given its charge state. Here decades of experience of solid state scientists studying such ions can be exploited. For a magnetic ion with an open $3d$ shell, the moment m (in μ_B) is $m=n_\uparrow-n_\downarrow$, the difference between spin $\uparrow$ and spin $\downarrow$ charges. The energy of an ion in the perovskite octahedral field is determined by the crystal field splitting $\Delta_{cf}=\varepsilon_{e_g}-\varepsilon_{t_{2g}}$ between e_g and t_{2g} levels, and the magnetic polarization energy $\frac{1}{4}I_{st}m^2$; in spin DFT the Stoner constant I_{st} gives the spin $\downarrow$ minus spin $\uparrow$ exchange splitting $\Delta_{ex}=I_{st}m$. Given the charge state d^n of an ion, where $n=n_\uparrow+n_\downarrow$, the energy balance is determined by the ratio I_{st}/Δ_{cf} and determines the moment m.

If one were interested only in magnetic insulators, it would probably be sufficient to incorporate the accumulated knowledge from solid state chemistry of transition metal ion charge states in perovskite oxides. However, in this search we are focussed on materials that are both metalliic (in one spin channel) and insulating (in the other channel). Indeed, the charge state of an ion (discussed in the previous subsection) becomes a tenuous concept. It is therefore important not only to ascertain the most probable value of the moment, but also whether there are likely to be other values that differ only a little in energy. Of course, banding that occurs in the solid plays an important role, at least in the metallic channel, and only the full calculation will answer the question.

The simple equations and plots of the resulting behavior are presented elsewhere [77] for two representative values of the ratio I_{st}/Δ_{cf}, that determines whether the ion takes on a high-spin or low-spin configuration. The conclusions of this exercise are straightforward to enumerate, and the results are familiar from inorganic chemistry classes:

- $S=\frac{5}{2}$ is attained only by a d^5 ion (viz. Mn^{2+}, Fe^{3+}, or Co^{4+}).
- $S=2$ occurs only for (high-spin) d^4 and d^6 ions.
- $S=\frac{3}{2}$ occurs only for d^3 and (high-spin) d^7 ions.
- $S=1$ is attained not only by d^2 and d^8 high-spin ions, but also by the low-spin d^4 ion $(t^3_{2g\uparrow}t^1_{2g\downarrow})$ if I_{st}/Δ_{cf} is small.
- $S=\frac{1}{2}$ occurs for low-spin d^5 and d^7 ions as well as for the single electron d^1 and single hole d^9 ions.

These results are for an isolated ion (in the crystal field). Within a crystal there are additional effects. (1) The kinetic energy, which results from inter-ionic hopping (via the intervening oxygen ion in the perovskite structure), tends to drive the moment away from integer values, sometimes with substantial effects as can be see below; (2) structural distortions (which were discussed above in a somewhat different context) lower symmetry, alter hopping amplitudes, and often lift orbital degeneracy; (3) there is the possibility of ions changing their charge state (determined by differences in

Table 1
Nominal charge states, Hund's rule (spin only) magnetic moments and crystal field (spin) moments m (in μ_B), for AMO_3 compounds

Compound	Ion	d^1	d^2	d^3	d^4	d^5	d^6	d^7	d^8	d^9
$A^{4+}M^{2+}O_3$	M^{2+}	(Sc)	Ti	V	Cr	Mn	Fe	Co	Ni	Cu
	m (no cf)	1	2	3	4	5	4	3	2	1
	m (cf)	1	2	3	4	5	0	1	2	1
$A^{3+}M^{3+}O_3$	M^{3+}	Ti	V	Cr	Mn	Fe	Co	Ni	(Cu)	
	m (no cf)	1	2	3	4	5	4	3	2	
	m (cf)	1	2	3	4	3	0	1	2	
$A^{2+}M^{4+}O_3$	M^{4+}	V	Cr	Mn	Fe	Co	(Ni)			
	m (no cf)	1	2	3	4	5	4			
	m (cf)	1	2	3	4	3	0			

Ions in parentheses are uncommon. As discussed in the text, Hund's rule will not be followed if the crystal field splitting is comparable to the intra-atomic exchange splitting. 'cf' and 'no cf' indicates atomic moments with a normal crystal field for the perovskite structure, or negligible crystal field (Hund's rule), respectively.

site energies and by intra-atomic repulsion). These effects are of course taken into account in self-consistent spin DFT calculations. However, the moments provided from the above list provide a good initial choice of ion pairs as candidates for an HM AFM.

3.2.4. Results for selected compounds

Compounds (i.e., ion pairs) were then chosen with the objective of achieving spin cancellation from two moments with equal spin S. In the following discussion, we refer to global spin directions by $\uparrow$ and $\downarrow$, while the terms 'majority' and 'minority' refer to each specific ion (spin channel that is more occupied, or less occupied) and does not specify a direction of the spin. Also, due to strong hybridization with the oxygen $2p$ states, it is not possible to specify an ionic moment precisely. Stated values provide the calculated (nominal) charge state and the (nominal) moment; often the actual calculated moment is not very close to an integer value. The calculations were carried out with an LAPW code [87,88].

$S=2$: Mn^{3+} d^4; Co^{3+} d^6. When the Mn and Co moments are anti-aligned, indeed an HM AFM state is obtained. Band effects are strong, and the moments in the ionic spheres are only $\approx 3\,\mu_B$ (rather than the $4\,\mu_B$ expected for $S=2$). The densities of states indicate [77] that the ionic picture is followed closely ($\Delta_{cf}=1.5$–2 eV, $\Delta_{ex}\approx 2$ eV). The conducting channel has 75% Co d, 25% Mn d character at the Fermi level. When the spins are aligned, high-spin Mn, low-spin Co resulted, reflecting the strong difference in hybridization that arises for FM alignment. The spin-aligned phase is 0.46 eV per M ion lower in energy than the HM AFM phase, so the sought-after HM AFM phase is at best metastable, and not a promising candidate.

$S=2$: $Cr^{3+}d^3$; $Fe^{3+}d^5$. This pair was chosen with the hope that differing charge states $[Cr^{2+}, Fe^{4+}: d^4, d^4]$ and equal $S=2$ spins would result. Two distinct solutions for anti-aligned moments were obtained, one with high-spin Fe ($4\,\mu_B$) parallel to the net moment, and the other with low-spin Fe ("$1\,\mu_B$") anti-aligned with the net moment. Both are HM; however, they are ferrimagnetic (FiM) with uncompensated spins. An FM, high-spin solution also was found. Of these three spin configurations, the high Fe spin FiM state is lowest in energy. All three states can be characterized as Cr^{3+}, Fe^{3+} (d^3, d^5) whose moments indeed are not expected to cancel.

$S=2$: $Cr^{3+}d^3$; $Ru^{3+}d^5$. The $4d$ Ru ion is isovalent with Fe, so this pair provides another possibility for an $S=2$ pair with unequal charges (Cr^{2+}, Ru^{4+}). However, like Cr–Fe, the Cr–Ru pair are found to be isovalent, and Ru is in its low-spin state. The compound is a HM FiM with a net moment of $2\,\mu_B$.

$S=\frac{3}{2}$: $Cr^{3+}d^3$; $Ni^{3+}d^7$. For small crystal field, the d^7 ion may be high spin ($3\,\mu_B$), thereby balancing the d^3 moment. For these pairs the anti-aligned configuration resulted in an FiM net moment of $0.60\,\mu_B$, near but not at the HM AFM result. The FM alignment is lower in energy by 0.15 eV per ion.

$S=1$: $Mn^{3+}d^4$; $V^{3+}d^2$. A low spin for Mn indeed resulted, for both anti-aligned and aligned moments. The densities of states are shown in Fig. 8; we discuss the unusual structure of the metallic channel below. The anti-aligned ordering results in an HM AFM state; moreover, this state is 0.17 eV/ion lower in energy than the FM alignment. Thus, this pair provides a good candidate for the HM AFM that this search hoped to locate.

$S=\frac{1}{2}$; $V^{4+}d^1$; $Cu^{2+}d^9$. Like for the $S=1$ case above, and unlike the other cases, the desired differing charge states are obtained for this pair. The differing ionic radii as well as the differing charge states of this pair of ions should give a strong preference for well-ordered structures (discussed more below). Both aligned and anti-aligned moment solutions were obtained, with *identical* energies. Moreover, the anti-aligned phase is an HM AFM. Owing to the identical energies of the different ordered alignments and their small spins, this system appears to be a possible candidate for a three-

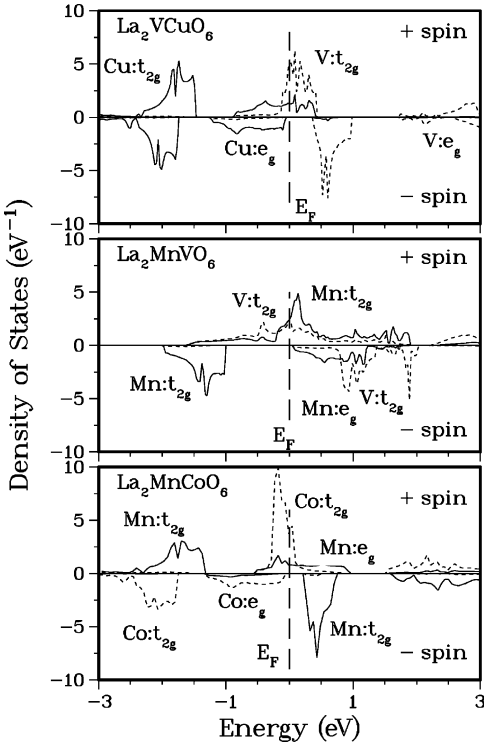

Fig. 8. Plots of the calculated atom- and symmetry-projected densities of states of the three HM AFM solutions discussed in the text. The two different spin directions are plotted above and below the line; the spin channel that is metallic is plotted above the line and is denoted "+", but recall there is no net spin moment in either direction. The DOS of one atom is plotted with a solid line, the other is plotted as dashed. The dominant character (t_{2g} or e_g) is noted. The widest gap, of about 1 eV, occurs for the Mn–V pair (middle panel). Interpretation of these spectral distributions is given in the text.

dimensional quantum magnetic system as $T \to 0$ (viz. heavy fermion metals, Kondo insulators), rather than a simple HM AFM or an exotic superconductor. (Note also that a disordered arrangement, such as a spin glass, might have a significantly different energy.) Structural relaxation should be considered, however.

It is worthwhile to return to the densities of states shown in Fig. 8 to interpret what can be learned from these plots. We concentrate first on the case of La_2MnCoO_6 (bottom panel), which is the most straightforward. For definiteness, let's refer to the "+ spin" of this plot as "up", then the Mn spin points up and the Co spin points down. Above the line, the Mn DOS (solid line) indicates that the majority spin Mn t_{2g} states are filled, while the e_g band crossing E_F is partially filled; *apparently* less than half-filled but one might call it half-filled, giving one more electron and a d^4 Mn configuration. The minority Mn states are empty. Below the line, the dashed lines indicate that the Co t_{2g} and e_g states are filled (exactly; they are below the gap). The Co minority t_{2g} states (which are '+'≡'*up*') are partially filled. However, the HM AFM character reflects the fact that the total number of 'up' and 'down' states are equal, and equal to five (this number is clear from the down spin DOS). The physical result is that the Mn majority e_g states and the Co minority t_{2g} states form a metallic band (for the 'up' spin direction) and their formal charges correspondingly become less clearly defined. The result is, however, most consistent with an Mn^{3+} (d^4), Co^{3+}(d^6) picture with compensating $S = 2$ moments. Some specific results are not so easily interpreted in the language of solid state chemistry (which is particularly adapted to insulators with clear charge states). The stated formal charges (given above) are only rough characterizations (and perhaps misleading if taken too seriously!) and, as noted, the calculated moments on Mn and Co are only around 3 μ_B (strict $S = 2$ would give moments of 4 μ_B). Band effects, where states are not readily associated with a specific ion, are substantial.

The V–Cu case (upper panel of Fig. 8) is not difficult to interpret: in the '+' spin direction there is one Cu e_g state *un*occupied, and one V t_{2g} state occupied, implying the charge states and $S = \frac{1}{2}$ as stated above. The Mn–V case, in the middle panel of Fig. 8, is much less straightforward to make sense of. These ions lie rather close in the periodic table, and their spins are low, so the exchange splitting and crystal field spittings are comparable. (For the Mn–Co case, exchange splitting dominated crystal field separation, while for the V–Cu case the opposite holds; either case simplifies the interpretation.) Nevertheless, the Mn^{3+} (d^4)–V^{3+} (d^2) specification makes the most sense.

Of these six pairs of transition metal ions in the double perovskite structure, three have led to at least a metastable HM AFM phase. This amount of success is remarkable considering there was previously not a single viable candidate. One of these is clearly only metastable (the Mn–Co pair) while Mn–V and V–Cu in the $LaT'T''O_3$ compound are not unstable towards ferromagnetic alignment of the moments. It must be said that there is no guarantee that all solutions of the equations (corresponding to local minima in the energy functional) have been obtained.

The calculated densities of states of these three states, shown in Fig. 8, reveal that qualitatively different types of gaps can occur in the insulating channel. The gap may separate d states on a single metal ion, or it may be of the "charge transfer" type where the gap lies between occupied d states on one ion and unoccupied d states on the other ion—the low energy electron-hole pair excitation then involves charge transfer between the two ions. The Mn–V compound (panel (b) of Fig. 8) has the gap separating Mn t_{2g} and e_g states (the band version of a Mott insulator). The Mn–Co and V–Cu compounds, on the other hand, have the charge transfer type of gap.

Building on these predictions, Park, Kwon, and Min have explored with similar calculations the double perovskite system $LaDVRuO_6$, where D is one of the *divalent* ions Ca, Sr, Ba [90]. This change alters the valence requirement to $Q + Q' = 7$, and opens up a new class of pairs of transition metal ions. It also complicates the synthesis process, since there is one more sublattice which should be ordered. Order on this sublattice may not be as important as on the transition metal sublattice; however, and in favorable cases the local strains imposed by the difference in these ions could assist ordering on the metal sublattice. Park et al. reported that both (111) ordering of the V and Ru ions (the order that is discussed above) and also (001) layering provide good HM AFM candidates.

3.2.5. *Experimental feedback*

Success (or not) of any such "design" of a material relies on subsequent experimental verification. We have made attempts to obtain experimental tests of these predictions. Around 1997 D. Chrisey and R. Stroud at the Naval Research Laboratory performed preliminary attempts to grow La_2MnVO_6 by pulsed laser deposition. Evidence of the double perovskite structure was not obtained; however, the attempts were not thorough because of the lack of funding to make a concerted study of the system. Initial attempts at fabrication are often not a good indication of optimal results.

Stimulated by our suggestion of La_2MnVO_6 as a possible HM AFM, Androulakis, Katsarakis, and Giapintzakis synthesized samples of La_2MnVO_6 by arc melting [91]. They obtained the desired cubic double perovskite structure, however ordering on the B sublattice was only partial. The observed magnetic behavior was suggested to be ferrimagnetic, although

no sharp onset was seen. Rather a smooth maximum in the susceptibility was observed around 10 K. Fitting of the inverse susceptibility in the 200–300 K range gave a Curie temperature $\Theta = -162$ K, and effective moment $p_{\text{eff}} = 5.8\ \mu_B$. Other magnetic measurements indicated spin-glass behavior, so the *B*-site disorder is probably dominating the behavior, thus providing no clear comparison (positive or negative) to the calculated predictions.

Although not directly related to our design effort in the $La_2TT'O_6$ system, very recent experimental work has appeared on the characterization of La_2MnCoO_{6-x}. The stoichiometric compound is in fact reported to be an FM insulator [92]. It is, however, sensitive to oxygen stoichiometry, and another phase is reported with a small concentration of oxygen vacancies ($x = 0.05$), where a lower symmetry structure and somewhat more conducting phase is found. Such experimental studies provide important information for the refinement of the design described here.

3.2.6. Evaluation of studies so far

Although the local spin density functional calculations used here generally give good charge densities and in a majority of systems (including metallic perovskites [89]) predict magnetic properties as well, several questions remain. Whether the proposed compounds can be made can be answered only by experiment; competing phases are too numerous to calculate. Magnetic moments, type of spin ordering, and ionic charges can be sensitive to volume and most calculations reported here were carried out only at the representative cubic perovskite lattice constant of 3.89 Å. However, variations of the volume for the Mn–V and V–Cu compounds confirmed that this volume is realistic (near the minimum of energy) and that the HM AFM phases persisted at nearby volumes. Relaxation of the positions of the O ions as allowed by symmetry (see Fig. 1) was carried out only for the Mn–V compound. The oxygen octahedron relaxed inward around the smaller Mn ion [93] by only 0.02 Å, further stabilizing the HM AFM state (that is, E_F moved toward the center of the gap). Structural distortions to lower symmetry structures should also be investigated.

A limitation of the local spin density functional calculations used here is the inability to predict whether transition metal compounds are correlated electron systems. In the La_2VCuO_6 compound, for example, the bandwidth of the conduction band at the Fermi energy of the HM AFM state is only 1 eV wide, and strong on-site repulsion (''Hubbard U'') of electrons will tend to drive the metallic channel insulating. If this occurs, it may provide an example of yet another new phenomenon in these systems: a case in which one spin channel is a Mott insulator while the other is better described as a band insulator, or possibly a charge-transfer insulator. An extension of the local spin density method, referred to as the LSDA + U method [94,95] often provides a vastly improved mean-field description of correlated insulators. However, at present it is at best questionable for application to metals, so its use is usually restricted to materials that are known to be insulators. Preliminary results from a new pseudopotential self-interaction corrected method introduced by Filippetti and Spaldin [96] suggest that it might offer significant improvements in DFT calculations for strongly correlated systems including magnetic metals.

In La_2MnVO_6, on the other hand, the bandwidth of the metallic channel is more than 3 eV wide, and correlation effects should be much less important. The distinctions in Fig. 8(b) are easy to understand. The Mn majority t_{2g} states lie lower than any V states, and also hybridize less weakly with O 2*p* states than do e_g states. Hopping within this band therefore must go Mn–O–O–Mn hence, the band is quite narrow (1 eV). The minority Mn t_{2g} states lie in the same range as the majority V t_{2g} states; however, since the ionic moments are antiparallel these states have the same spin direction (+ in Fig. 3(b)) and can form a mutual, relatively broad, band based on Mn–O–V–O–Mn–⋯ hopping. Occupation of this comparatively broad band results in cancellation of part of the Mn moment. This reduced moment results (self-consistently) in reduced exchange splitting and leads to the low-spin Mn moment. Hence, it is reasonable to expect the conducting character of this band to survive correlation corrections.

An example of a spin density for an HM AFM phase is shown in Fig. 9 for the V–Cu compound. The spin-density isosurfaces illustrate very graphically the difference between the up and down spin densities, particularly the difference in the sizes of the V^{4+} and Cu^{2+} ions. Unlike conventional perovskite antiferromagnets where the oxygen is polarized only in a dipole form with no net moment, here the O ion has a net moment that lies in the same direction as the Cu spin. This unusual form of spin density for an AFM should be more readily apparent in the magnetic form factor measured in polarized neutron scattering experiments [97] than in the typical case in which there is no net moment on the O ion.

3.2.7. Comments

This example of a computational design of an HM AFM indeed indicates that the double perovskite class of compounds provides a fertile environment for good candidates for this new type of magnetic material. Although this search was confined to the La *A*-site cation (which may be considered representative of trivalent cations), mixed cation compounds such as $A^{2+}B^{3+}M'M''O_6$ show strong tendencies to form ordered structures and may also provide good candidates. Divalent cations in the double perovskite structure should be given a close look. The choice of

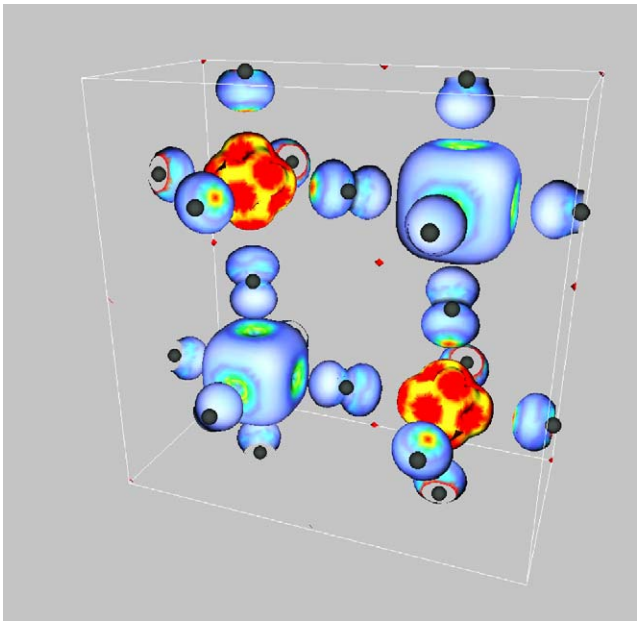

Fig. 9. Isocontour plot of the magnetization density of the HM AFM state calculated for La_2VCuO_6. The red–yellow surface surrounds the Cu^{2+} ion, while the larger blue surface surrounds the V^{4+} ion; the spin directions are opposite but the magnetization of the spin densities are the same on these surfaces. The other blue surfaces illustrate the polarization of oxygen 2*p* states, which is in the same direction as the Cu spin. The color is determined by the magnitude of the gradient of the spin density, not by the direction of spin. Two of the double perovskite unit cells are pictured (from Ref. [77]).

the double perovskite class should not be interpreted as suggesting that perovskites provide the most likely possibility; certainly other crystal structures deserve strong consideration. The important lesson here is that it should not be a formidable problem to design and synthesize HM AFM compounds, so the study of their myriad unusual properties may begin.

4. Summary and future work

In this overview, we have illustrated a general scheme which can be used in the first principles computational design of new materials, and described its application to two examples: the design of a magnetoelectric multiferroic, and the search for a half-metallic antiferromagnet. We believe that these examples illustrate that computational predictions should take a place alongside experimental exploration in the design of new materials.

Certainly the application of first principles computational design is not restricted to the classes of materials that we have described here. Other materials that might be particularly amenable to DFT design include novel giant magnetoresistive (GMR) materials [98,99] and improved spintronic materials [100] such as diluted magnetic semiconductors with higher Curie temperatures and magnetostrictive materials with larger coupling constants, to name just two.

Acknowledgments

Funding for this work was provided by the National Science Foundation's Division of Materials Research, Grant numbers DMR-0312407 and DMR-0114818. The earlier work of W.E.P. was supported by the Office of Naval Research. This work made use of the UCSB MRL's Central Facilities supported by the National Science Foundation under award No. DMR00-80034.

References

[1] R.B. Woodward, R. Hoffmann, The conservation of orbital symmetry, Academic Press, New York, 1970.
[2] E. Wimmer, Mater. Sci. Eng. B 37 (1996) 72–82.
[3] N.N. Kiselyova, V.P. Gladun, N.D. Vashchenko, J. Alloys Compd. 279 (1988) 8–13.
[4] http://www.kluweronline.com/jrnltoc.htm/0928-1045
[5] H. Hohenberg, W. Kohn, Phys. Rev. 136 (1964) 864–871.
[6] W. Kohn, L.J. Sham, Phys. Rev. 140 (1965) 1133–1138.
[7] M.T. Yin, M.L. Cohen, Phys. Rev. B 26 (1982) 5668–5686.
[8] J. Neugebauer, M. Scheffler, Phys. Rev. B 46 (1992) 16067–16080.
[9] U. von Barth, L. Hedin, J. Phys. C 5 (1972) 1629.
[10] M. Schlüter, L.J. Sham, Phys. Today 2 (1982) 36–43.
[11] D. Singh, Planewaves, Pseudopotentials and the LAPW Method, Kluwer, Dordrecht, 1994, 115pp.
[12] M.C. Payne, M.P. Teter, D.C. Allan, T.A. Arias, J.D. Joannopoulos, Rev. Mod. Phys. 64 (1992) 1045–1097.
[13] R.O. Jones, O. Gunnarsson, Rev. Mod. Phys. 61 (1989) 689–746.
[14] W.E. Pickett, Comput. Phys. Rep. 9 (1989) 115–198.
[15] P. Bendt, A. Zunger, Phys. Rev. Lett. 50 (1983) 1684–1688.
[16] X. Gonze, Phys. Rev. B 55 (1997) 10337–10354.
[17] S. Baroni, S. de Gironcoli, A. Dal Corso, Rev. Mod. Phys. 73 (2001) 515.
[18] M.L. Cohen, Phys. Today 32 (1979) 40–47 and references therein.
[19] S.G. Louie, S. Froyen, M.L. Cohen, Phys. Rev. B 26 (1982) 1738–1742.
[20] D. Sánchez-Portal, P. Ordejón, E. Artacho, J.M. Soler, Int. J. Quant. Chem. 65 (1997) 453–461.
[21] J.M. Soler, E. Artacho, J.D. Gale, A. García, J. Junquera, P. Ordejón, D. Sánchez-Portal, J. Phys.: Condens. Matter 14 (2002) 2745–2779.
[22] http://www.uam.es/departamentos/ciencias/fismateriac/siesta
[23] O.K. Anderson, Phys. Rev. B 12 (1975) 3060.
[24] The ABINIT code is a common project of the Universite Catholique de Louvain, Corning Incorporated, and other contributors (URL http://www.pcpm.ucl.ac.be/abinit).
[25] http://spinor.sourceforge.net
[26] http://www.gnu.org/copyleft/gpl.txt
[27] http://cst-www.nrl.navy.mil/singh/acres/info.html
[28] http://www.llnl.gov/CASC/sc2001_fliers/FPMD/FPMD01.html
[29] http://www.cpmd.org/
[30] http://cst-www.nrl.navy.mil/people/singh/planewave/
[31] http://www.fhi-berlin.mpg.de/th/fhimd/
[32] http://cms.mpi.univie.ac.at/vasp/
[33] http://www.accelrys.com

[34] M.C. Payne, X. Weng, B. Hammer, G. Francis, U. Bertram, A. de Vita, J.S. Lin, V. Milman, A. Qteish, unpublished.
[35] P. Blaha, K. Schwarz, J. Luitz, in: K. Schwarz (Ed.), WIEN97, A Full Potential Linearized Augmented Plane Wave Package for Calculating Crystal Properties, Technical University of Wien, Vienna, 1999, ISBN 3-9501031-0-4.
[36] http://www.flapw.de/fleurhaupt.html
[37] http://www.princeton-tech.com/index.html; alternatively, see links from http://www.mpi-stuttgart.mpg.de/andersen/
[38] http://www.ifw-dresden.de/agtheo/FPLO/
[39] http://www.mpi-stuttgart.mpg.de/andersen/LMTODOC/LMTODOC.html
[40] B. Silvi, A. Savin, Nature 371 (1994) 683.
[41] H. Schmid, Ferroelectrics 162 (1994) 317–338.
[42] C. Bernard, J.L. Tallon, Ch. Niedermayer, Th. Blasius, A. Golnik, E. Brücher, R.K. Kremer, D.R. Noakes, C.E. Stronach, E.J. Anslado, Phys. Rev. B 59 (1999) 14099–14107.
[43] S. Saxena, Nature 406 (2000) 587.
[44] D. Aoki, A. Huxley, E. Ressouche, D. Braithwaite, J. Flouquet, J.-P. Brison, E. Lhotel, C. Paulsen, Nature 413 (2001) 613–616.
[45] W.E. Pickett, R. Weht, A.B. Shick, Phys. Rev. Lett. 83 (1999) 3713–3716.
[46] C. Pfleider, H. Löhneysen, J. Low Temp. Phys. 126 (2002) 933–947.
[47] I.J. Busch-Vishniac, Phys. Today 56 (7) (1998) 28–34.
[48] V.E. Wood, A.E. Austin, in: A.J. Freeman, H. Schmid (Eds.), Magnetoelectric Interaction Phenomena in Crystals, Gordon and Breach, London, 1975.
[49] R.E. Cohen, J. Phys. Chem. Sol. 61 (2001) 139–146.
[50] R.D. King-Smith, D. Vanderbilt, Phys. Rev. B 47 (1993) 1651.
[51] R. Resta, Phys. Rev. Lett. 77 (1996) 2265–2269.
[52] G. Ortiz, R.M. Martin, Phys. Rev. B 49 (1994) 14202.
[53] K.M. Ok, N.S.P. Bhuvanesh, P.S. Halasyamani, Inorg. Chem. 40 (2001) 1978.
[54] R.E. Cohen, H. Krakauer, Ferroelectrics 136 (1992) 95.
[55] R.E. Cohen, Nature 358 (1992) 136–138.
[56] M. Atanasov, D. Reinen, J. Phys. Chem. A 105 (2001) 5450–5467.
[57] U.V. Waghmare, N.A. Spaldin, H.C. Kandpal, R. Seshadri, Phys. Rev. B 67 (2003) 125111.
[58] P. Weiss, J. Phys. 6 (1907) 661.
[59] E.C. Stoner, Philos. Mag. 15 (1933) 1080.
[60] H.J.F. Jansen, Phys. Today 48 (4) (1995) 50–55.
[61] N.A. Hill, J. Phys. Chem. B 104 (2000) 6694–6709.
[62] N.A. Hill, Ann. Rev. Matter. 32 (2002) 1.
[63] I. Sosnowska, T.P. Neumaier, E. Steichele, J. Phys. C 15 (1982) 4835–4839.
[64] Y.F. Popov, A.K. Zvezdin, G.P. Vorob'ev, A.M. Kadomtseva, V.A. Murashev, D.N. Rakov, JETP Lett. 57 (1993) 69–71.
[65] F. Sugawara, S. Iiida, Y. Syono, S. Akimoyo, J. Phys. Soc. Jpn. 25 (1968) 1553–1558.
[66] S. Vasudevan, C.N.R. Rao, A.M. Umarji, G.V. Subba Rao, Mater. Res. Bull. 14 (1979) 451–454.
[67] Y.Y. Tomashpol'skii, Y.N. Venevtsev, Sov. Phys. Cryst. 16 (1972) 905–908;
V.A. Bokov, N.A. Grigoryan, M.F. Bryzhina, V.S. Kazaryan, Bull. Acad. Sci. USSR 33 (1969) 1082–1084;
F. Sugawara, S. Iiida, Y. Syono, S. Akimoyo, J. Phys. Soc. Jpn. 25 (1968) 1553–1558;
V.A. Bokov, I.E. Myl'nikova, S.A. Kizhaev, M.F. Bryzhina, N.A. Grigoryan, Sov. Phys. Solid State 7 (1966) 2993–2994.
[68] J.B. Goodenough, Phys. Rev. 100 (1955) 564–573.
[69] N.A. Hill, K.M. Rabe, Phys. Rev. B 59 (1999) 8759–8769.
[70] R. Seshadri, N.A. Hill, Chem. Matter. 13 (2001) 2892–2899.
[71] T. Atou, H. Chiba, K. Ohoyama, Y. Yamaguchi, Y. Syono, J. Solid State Chem. 145 (1999) 639–642.
[72] U.V. Waghmare, N.A. Spaldin, H.C. Kandpal, R. Seshadri, Phys. Rev. B 67 (2003) 125111.
[73] H. Faqir, A. Chiba, M. Kikuchi, Y. Syono, M. Mansori, P. Satre, A. Sebaoun, J. Solid State Chem. 142 (1999) 113–119.
[74] A.M. dos Santos, S. Parahar, A.R. Raju, Y.S. Zhao, A.K. Cheetham, C.N.R. Rao, Solid State Commun. 122 (2002) 49–52.
[75] A.M. dos Santos, A.K. Cheetham, T. Atou, Y. Syono, Y. Yamaguchi, K. Ohoyama, H. Chiba, C.N.R. Rao, Phys. Rev. B 66 (2002) 064425-1-4.
[76] E. Ohshima, Y. Saya, M. Nantoh, M. Kawai, Solid State Commun. 116 (2000) 73–76.
[77] W. Pickett, Phys. Rev. B 57 (1998) 10613–10619.
[78] W.E. Pickett, J.S. Moodera, Phys. Today 54 (5) (2001) 39–44.
[79] H. van Leuken, R.A. de Groot, Phys. Rev. Lett. 74 (1995) 1171.
[80] W.E. Pickett, Phys. Rev. Lett. 77 (1996) 3185–3188.
[81] R.E. Rudd, W.E. Pickett, Phys. Rev. B 57 (1998) 557.
[82] V. Yu. Irkhin, M.I. Katsnel'son, Usp. Fiz. Nauk 164 (1994) 705; V. Yu. Irkhin, M.I. Katsnel'son, Sov. Phys. Usp. 37 (1994) 659.
[83] H. Eschrig, W.E. Pickett, Solid State Commun. 118 (2001) 123–127.
[84] M.T. Anderson, et al., Prog. Solid State Chem. 22 (1993) 197.
[85] D.J. Singh, W.E. Pickett, Phys. Rev. B 53 (1996) 1146–1160.
[86] K.-I. Kobayashi, T. Kimura, H. Sawada, K. Terakura, Y. Tokura, Nature 395 (1998) 677.
[87] S.H. Wei, H. Krakauer, Phys. Rev. Lett. 55 (1985) 1200–1203.
[88] D.J. Singh, Phys. Rev. B 43 (1991) 6388.
[89] D.J. Singh, W.E. Pickett, Phys. Rev. B 57 (1996) 88–91.
[90] J.H. Park, S.K. Kwon, B.I. Min, Phys. Rev. B 65 (2002) 174401.
[91] J. Androulakis, N. Katsarakis, J. Giapintzakis, cond-mat/0206146 (2002).
[92] R.I. Dass, J.B. Goodenough, Phys. Rev. B 67 (2003) 014401.
[93] R.D. Shannon, C.T. Prewitt, Acta Crystallogr. 25 (1969) 925.
[94] V.I. Anisimov, F. Aryasetiawan, A.I. Lichtenstein, J. Phys.: Condens Matter 9 (1997) 767–808.
[95] A.B. Shick, A.I. Liechtenstein, W.E. Pickett, Phys. Rev. B 60 (1999) 10763–10769.
[96] A. Filippetti, N.A. Spaldin, Phys. Rev. B 67 (2003) 125109.
[97] J.W. Lynn, G. Shirane, M. Blume, Phys. Rev. Lett. 37 (1976) 154–157.
[98] M.N. Baibich, J.M. Broto, A. Fert, F. Nguyen Van Dau, F. Petroff, P. Etienne, G. Creuzet, A. Friederich, J. Chazelas, Phys. Rev. Lett. 61 (1988) 2472–2475.
[99] C. Felser, K. Ahn, R.K. Kremer, R. Seshadri, A. Simon, J. Sol. State Chem. 147 (1999) 19;
C. Felser, R. Seshadri, Int. J. Inorg. Mater. (Raveau FestSchrift) 2 (2000) 677.
[100] H. Ohno, Science 281 (1998) 951–956.